Hindawi Publishing Corporation
International Journal of Antennas and Propagation
Volume 2009, Article ID 390782, 8 pages
doi:10.1155/2009/390782

Research Article

Efficient Time-Domain Ray-Tracing Technique for the Analysis of Ultra-Wideband Indoor Environments including Lossy Materials and Multiple Effects

F. Saez de Adana,[1] O. Gutiérrez,[1] M. A. Navarro,[1] and A. S. Mohan[2]

[1] *Departamento de Ciencias de la Computación, Escuela Politécnica, Universidad de Alcalá, Campus Universitario, 28806 Alcalá de Henares, Spain*
[2] *Faculty of Engineering, University of Technology Sydney, P.O. Box 123, Broadway, NSW 2007, Australia*

Correspondence should be addressed to F. Saez de Adana, kiko.saez@uah.es

Received 30 June 2009; Revised 10 November 2009; Accepted 11 December 2009

Recommended by Stefano Selleri

This paper presents an efficient application of the Time-Domain Uniform Theory of Diffraction (TD-UTD) for the analysis of Ultra-Wideband (UWB) mobile communications for indoor environments. The classical TD-UTD formulation is modified to include the contribution of lossy materials and multiple-ray interactions with the environment. The electromagnetic analysis is combined with a ray-tracing acceleration technique to treat realistic and complex environments. The validity of this method is tested with measurements performed inside the Polytechnic building of the University of Alcala and shows good performance of the model for the analysis of UWB propagation.

1. Introduction

Ultra-wideband (UWB) technology has developed rapidly in the past several years. This technology is especially attractive in high data rate and short-range wireless communications. These applications make UWB technology suitable for indoor mobile communications applications, such as wireless personal-area networks (WPANs). This interest has motivated the study of the propagation of the UWB signals in indoor environments as an important task for the implementation of the WPANs.

In the last decades, significant effort has been focused on the characterization of the indoor channel for narrowband systems. The statistical [1–4] and deterministic [5–8] models have been most frequently used in these studies. The deterministic models are mostly based on the ray-tracing techniques [5–7] to predict the multipath phenomena, and the Uniform Theory of Diffraction (UTD) technique [9] to calculate the received power or the propagation losses. However, the features of the UWB systems (with bandwidth in the range of the GHz) render the conventional narrowband propagation models, both statistical and deterministic, not applicable. These models are mostly based on frequency-domain analysis while UWB requires a time-domain analysis, due to its wide bandwidth. Therefore, special models must be used to predict the signal propagation in UWB systems. Although statistical models have been proposed [10, 11], they are not adequate, as multipath propagation produces a strong fast-fading on the indoor propagation for UWB systems which is not accurately predicted by the statistical models. Regarding the deterministic models, the frequency domain UTD can be applied, performing an analysis at several frequencies and obtaining the time response using an Inverse Fourier Transform. However, this procedure is computationally inefficient by comparison to a direct analysis in time domain.

Instead, Time-Domain Uniform Theory of Diffraction (TD-UTD) was developed to obtain the solution in the time domain for the reflection and the diffraction of a transient electromagnetic wave. The inclusion of the multipath phenomena in this theory, and the analysis in the TD makes this technique suitable for UWB applications. TD-UTD was

firstly developed by Vemttipong and Kouyoumjian [12] who applied the inverse Laplace transform to the frequency-domain UTD formulation. Later, Rousseau and Pathak [13] presented closed-form solutions for the diffraction by an edge, by modifying the formulation presented in [12]. The results obtained in [13] can be directly applied to develop a method for the calculation of the indoor propagation in UWB systems.

The formulation presented in [13] has been modified in this paper to introduce the contribution of lossy materials, which form the indoor environment in the reflection, transmission and diffraction. The idea is to obtain the reflection, transmission or diffraction coefficients using an Analytical Time Transform (ATT) from their expressions in the frequency domain. In addition, multiple interactions are also considered in the approach. These interactions included multiple reflections and transmissions, and the interactions between reflected and diffracted rays. Hence, both reflection-diffraction and diffraction-reflection interactions are included. These interactions, which are obtained in the frequency domain from the product of the coefficients involved in the propagation mechanisms, can also be computed in the time domain by convolving those coefficients instead.

The ray-tracing associated with the computation of the transient response does not change with respect to the ray-tracing in the frequency domain. The technique developed by the authors in [5] applied to the frequency domain is also used in this approach. The main advantage of that method is the inclusion of a novel ray-tracing acceleration technique called the Angular Z-Buffer (AZB). This technique, as can be shown in [5, 14], reduces the computation time associated to the ray-tracing by several orders of magnitude. Therefore, the analysis of complex and realistic environments can now be computed much more quickly.

Other TD-UTD models have also been proposed in the past. In [15], Yao proposed a TD-UTD model that included the contributions of direct, reflected and diffracted rays, in addition to the transmitted ray in [16]. A simulator based on TD-UTD for indoor UWB propagation was presented in [17]. The work in [18] took into account the polarization of both the transmitted and the received antennas by investigating a model consisting of two cube-like objects. The method proposed in this work improves on these previous approaches by generalizing the TD-UTD formulation for the analysis of realistic environments. This aim is achieved by including the multiple-ray contributions. Moreover, the electromagnetic formulation is combined with a previously-developed ray-tracing acceleration technique to reduce the computational cost for analysis of these realistic environments. Finally, with the aim of further reducing this computation time, the convolution of the analytical impulse response with the excitation is performed in an efficient way by expressing the excitation waveform as a sum of simple expansion functions thus allowing the convolution to be performed in closed form.

Taking these into account, the analysis of a real site has been performed to prove the validity of the model and its ability to analyze realistic environments. Some experimental measurements have been performed and comparisons with the predictions of the proposed model are presented in this paper. The analysis of such a complex site was made possible due to the improvements included in our approach.

2. TD-UTD Model for Indoor Propagation

As shown in Figure 1, the classical UTD in the frequency domain obtains the field at an observation point inside an indoor environment as the sum of the contribution of different rays. These rays that started from the source (S) reached that observation point (O) either directly or after one or several reflections, diffractions, transmissions or the multiple combinations of these effects. Accordingly, the TD-UTD analytical impulse response in that environment can be obtained from an ATT, which consisted of a one-sided Inverse Fourier Transform (IFT) of the frequency response, as can be seen in [12, 13], and can be written as:

$$\begin{aligned} \overset{+}{f}_I(t) = {} & \overset{+}{f}_I^{\,i}(t) + \overset{+}{f}_I^{\,r}(t) + \overset{+}{f}_I^{\,t}(t) + \overset{+}{f}_I^{\,d}(t) + \overset{+}{f}_I^{\,\mathrm{mr}}(t) \\ & + \overset{+}{f}_I^{\,\mathrm{mt}}(t) + \overset{+}{f}_I^{\,\mathrm{rd}}(t) + \overset{+}{f}_I^{\,\mathrm{dr}}(t), \end{aligned} \tag{1}$$

where $\overset{+}{f}_I^{\,i}(t)$, $\overset{+}{f}_I^{\,r}(t)$, $\overset{+}{f}_I^{\,t}(t)$, $\overset{+}{f}_I^{\,d}(t)$, $\overset{+}{f}_I^{\,\mathrm{mr}}(t)$, $\overset{+}{f}_I^{\,\mathrm{mt}}(t)$, $\overset{+}{f}_I^{\,\mathrm{rd}}(t)$, and $\overset{+}{f}_I^{\,\mathrm{dr}}(t)$ are the analytical signal representations for the direct field $\overset{+}{f}_I^{\,i}(t)$, reflected field $\overset{+}{f}_I^{\,r}(t)$, transmitted field $\overset{+}{f}_I^{\,t}(t)$, diffracted field $\overset{+}{f}_I^{\,d}(t)$, multiply reflected field $\overset{+}{f}_I^{\,\mathrm{mr}}(t)$, multiply transmitted $\overset{+}{f}_I^{\,\mathrm{mt}}(t)$, reflected-diffracted-field $\overset{+}{f}_I^{\,\mathrm{rd}}(t)$ and diffracted-reflected field $\overset{+}{f}_I^{\,\mathrm{dr}}(t)$, respectively. Therefore, the impulse response as shown in (1) included all the multipath phenomena as mentioned previously. Each term in (1) will be described in the following sections.

2.1. Direct Field. The contribution of the direct field to the impulse response is obtained as the ATT of the usual Geometrical Optics (GO) incident field and can be expressed by the following equation [13]:

$$\overset{+}{f}_I^{\,i}(t) = E_0^i |A_i(s_i)| \overset{+}{\delta}\left(t - \frac{s_i}{c}\right) \tag{2}$$

where E_0^i is the initial field value, which is constant with time and frequency, $A_i(s_i)$ is the spreading (or spatial divergence) factor for the direct ray, and s_i is the distance between the source and the observation point. The spreading factor for the direct ray is given by [13]:

$$A_i(s_i) = \sqrt{\frac{\rho_1^i \rho_2^i}{\left(\rho_1^i + s_i\right)\left(\rho_2^i + s_i\right)}} \tag{3}$$

where ρ_1^i and ρ_2^i are the principal radii of curvature of the incident wavefront at the observation point (see Figure 2).

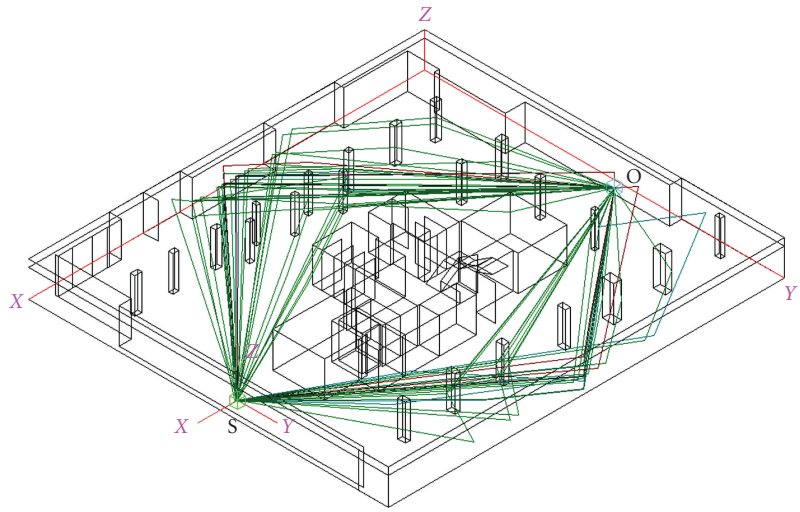

Figure 1: Ray-tracing mechanisms between a given source (S) and an observer (O). The figure shows the complexity of the multipath phenomenon in an indoor environment.

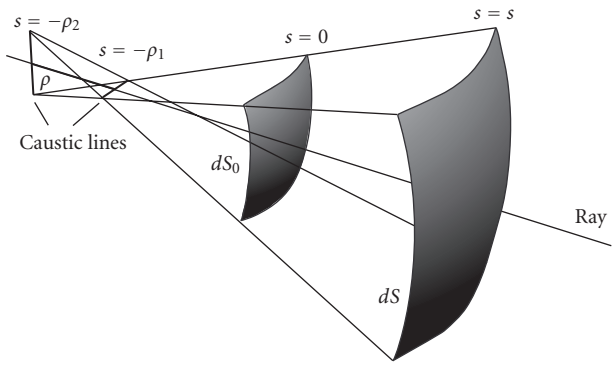

Figure 2: Incident ray wavefront.

2.2. Reflected Field. Similar to the case of the direct field, the contribution of the reflected field to the impulse response is obtained from the ATT of the classical GO expression in the frequency domain by the following equation:

$$\overset{+}{f}{}_I^r(t) = E_0^i \overset{+}{R}\left(t - \frac{s_i}{c} - \frac{s_r}{c}\right)|A_i(s_i)A_r(s_r)|, \tag{4}$$

where s_i is, in this case, the distance between the source and the reflection point, s_r is the distance between the reflection point and the observation point, $A_r(s_r)$ is the spreading (or spatial divergence) factor for the reflected ray which is expressed as [13]

$$A_r(s_r) = \sqrt{\frac{\rho_1^r \rho_2^r}{(\rho_1^r + s_r)(\rho_2^r + s_r)}}, \tag{5}$$

where ρ_1^r and ρ_2^r are the principal radii of curvature of the reflected wavefront at the observation point.

In (4), $\overset{+}{R}(t)$ is the TD dyadic reflection coefficient which must be expressed in terms of its vertical and parallel components. These coefficients are obtained as the ATT of the classical Fresnel reflection coefficients [15] for a reflected surface composed by a lossy material. By performing this ATT, the parallel component can be expressed as

$$\overset{+}{R}_{\parallel}(t) = K\overset{+}{\delta}(t) + \frac{4\kappa}{1-\kappa^2}\frac{e^{-at}}{t}\sum_{n=1}^{\infty}(-1)^{n+1}nK^nI_n(at), \tag{6}$$

where I_n is the modified Bessel function of order n and

$$K = \frac{1-\kappa}{1+\kappa}, \quad \kappa = \frac{\sqrt{\varepsilon_r - \cos^2\phi}}{\varepsilon_r \sin\phi}, \quad a = \frac{120\pi\sigma c}{2\varepsilon_r} \tag{7}$$

and the perpendicular component is as follows

$$\overset{+}{R}_{\perp}(t) = -\left[K\overset{+}{\delta}(t) + \frac{4\kappa}{1-\kappa^2}\frac{e^{-at}}{t}\sum_{n=1}^{\infty}(-1)^{n+1}nK^nI_n(at)\right], \tag{8}$$

where in this case,

$$\kappa = \frac{\sin\phi}{\sqrt{\varepsilon_r - \cos^2\phi}}, \quad a = \frac{120\pi\sigma c}{2\varepsilon_r\left(1 - \dfrac{\cos^2\phi}{\varepsilon_r}\right)} \tag{9}$$

and the rest of parameters are the same.

2.3. Transmitted Field. The impulse response for the transmitted field is analogous to the response for the reflected field and can be written as:

$$\overset{+}{f}{}_I^r(t) = E_0^i \overset{+}{T}\left(t - \frac{s_i}{c} - \frac{s_t}{c}\right)|A_i(s_i)A_t(s_t)|, \tag{10}$$

where s_i is, in this case, the distance between the source and the transmission point, s_t is the distance between the transmission point and the observation point, $A_t(s_t)$ is the spreading (or spatial divergence) factor for the transmitted

ray that can be obtained using expression (5) by replacing the radii of curvature of the reflected wavefront by those of the transmitted wavefront, and $\overset{+}{\overline{T}}(t)$ is the TD dyadic transmission coefficient, which must be also expressed in terms of its vertical and parallel components. The transmission coefficient can be easily obtained by considering that the relationship between the reflection and the transmission coefficients is the same in the time domain than as in in the frequency domain, and is given by

$$\overset{+}{\overline{T}}(t) = I + \overset{+}{\overline{R}}(t), \tag{11}$$

where I is the identity matrix.

2.4. Diffracted Field. In the case of diffraction, its contribution to the impulse response is given by the ATT of the UTD expression for the frequency domain as follows:

$$\overset{+}{f}{}_I^d(t) = E_0^i \overset{+}{D}\left(t - \frac{s_i}{c} - \frac{s_d}{c}\right)|A_i(s_i)A_d(s_d)|, \tag{12}$$

where s_i is, in this case, the distance between the source and the diffraction point, s_d is the distance between the diffraction point and the observation point, $A_d(s^d)$ is the spreading (or spatial divergence) factor for the reflected ray given by [13]

$$A_d(s_d) = \sqrt{\frac{\rho^s}{(\rho^s + s_d)\cdot s_d}}, \tag{13}$$

where ρ^s is the principal radius of curvature of the diffracted wavefront at the observation point.

On the other hand, $\overset{+}{\overline{D}}(t)$ is the TD dyadic diffraction coefficient, which must be expressed in terms of its components with respect to the edge-fixed system. The diffraction coefficients for a PEC wedge are obtained as the sum of four terms as in [13]. If the lossy materials are included in the formulation, the last two terms corresponding to the contribution of the reflected shadow boundary must include the effect of the lossy reflection coefficient. In the frequency domain, this is performed by a product. Therefore, the convolution between the reflection coefficient and these two terms of the diffraction coefficient must instead be performed in the time domain. Performing this convolution results in the following expression for the diffraction coefficients:

$$\overset{+}{\overline{D}}_{\beta,\phi}(t) = \overset{+}{D}_1(t) + \overset{+}{D}_2(t) + \overset{+}{\overline{R}}_{\perp,\parallel} * \left[\overset{+}{D}_3(t) + \overset{+}{D}_4(t)\right]. \tag{14}$$

The expressions for $\overset{+}{D}_1(t)$, $\overset{+}{D}_2(t)$, $\overset{+}{D}_3(t)$ and $\overset{+}{D}_4(t)$ are given as follows [13]:

$$\begin{aligned}
\overset{+}{D}_1(t) &= A_0\cot\left[\frac{\pi + (\phi - \phi')}{2n}\right]\overset{+}{F}\left[L^i a^+(\phi - \phi')\right],\\
\overset{+}{D}_2(t) &= A_0\cot\left[\frac{\pi - (\phi - \phi')}{2n}\right]\overset{+}{F}\left[L^i a^-(\phi - \phi')\right],\\
\overset{+}{D}_3(t) &= A_0\cot\left[\frac{\pi + (\phi + \phi')}{2n}\right]\overset{+}{F}\left[L^{rn} a^+(\phi + \phi')\right],\\
\overset{+}{D}_4(t) &= A_0\cot\left[\frac{\pi - (\phi + \phi')}{2n}\right]\overset{+}{F}\left[L^{ro} a^-(\phi + \phi')\right],
\end{aligned} \tag{15}$$

with $A_0 = -1/(2n\sqrt{2\pi}\sin\beta_0^i)$ where β_0^i is the angle between the direction of incidence and the vector of the edge and $\overset{+}{F}(x,t) = \sqrt{x/\pi}(j\sqrt{t} + \sqrt{x/c})/\sqrt{t}(t + x/c)$.

The L^i are distance parameters associated with the incident shadow boundaries and are the same in the frequency domain. These parameters are given by

$$L^i = \frac{s_d(\rho_e^i + s_d)\rho_1^i\rho_2^i}{\rho_e^i\left(\rho_1^i + s_d\right)\left(\rho_2^i + s_d\right)}\sin^2\beta_0^i, \tag{16}$$

$$L^{ro,n} = \frac{s_d(\rho_e^{ro,n} + s_d)\rho_1^{ro,n}\rho_2^{ro,n}}{\rho_e^{ro,n}(\rho_1^{ro,n} + s_d)(\rho_2^{ro,n} + s_d)}\sin^2\beta_0^i, \tag{17}$$

where ρ_1^i is the radii of curvature 1 of the incident wavefront at the edge, ρ_2^i is the radii of curvature 2 of the incident wavefront at the edge, ρ_e^i is the radii of curvature of the incident wavefront at edge-fixed plane of incidence, $\rho_1^{ro,rn}$ is the radii of curvature 1 of the reflected wavefront from the o and n faces, respectively, $\rho_2^{ro,rn}$ is the radii of curvature 2 of the reflected wavefront from the o and n faces, respectively, and $\rho_e^{ro,rn}$ is the radii of curvature of the reflected wavefront from in the plane containing the reflected ray and the edge.

The function $a^\pm$ of the expressions (15) is given by

$$\begin{aligned}
a^\pm(\beta^\pm) &= 2\cos^2\left(\frac{2n\pi N^\pm - \beta^\pm}{2}\right),\\
\beta^\pm &= \phi^d \pm \phi^i,\\
2\pi n N^+ - \left(\phi^d \pm \phi^i\right) &= \pi,\\
2\pi n N^- - \left(\phi^d \pm \phi^i\right) &= -\pi.
\end{aligned} \tag{18}$$

The geometrical parameters involved in the calculation of the diffraction coefficients are the same as in the frequency domain as shown in Figure 3 and are explained in [9].

2.5. Multiple Reflected and Multiple Transmitted Fields. The expressions for the m-order reflections and transmissions are easily derived recursively from the first order effects. For instance, the second-order reflection will be a single reflection where the source is set as the first reflection point and the incident field is the simple reflected field. Using this

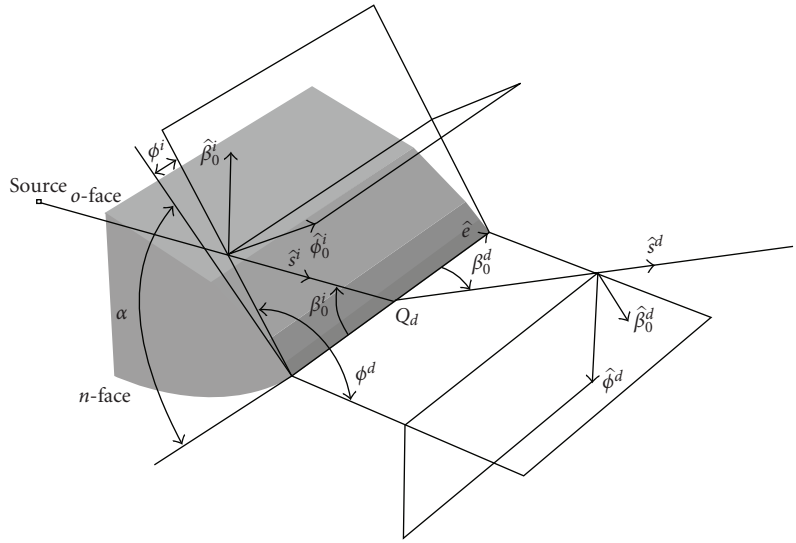

FIGURE 3: Geometrical parameters and edge-fixed system for the diffracted ray. In the figure $\hat{e}$ is the vector of the edge, Q_d is the diffraction point, $\hat{s}^i$ and $\hat{s}^d$ are the incident and diffraction directions, respectively, β_0^i, β_0^d, ϕ^i and ϕ^d ($\beta_0^i = \beta_0^d = \beta_0$) are the diffraction angles and $\hat{\beta}_0^i, \hat{\phi}^i$ and $\hat{\beta}_0^d, \hat{\phi}^d$ are the vectors of the edge-fixed system necessary to apply the diffraction coefficients. All these parameters are explained in [9], because they are the same to the frequency domain case.

recursion, an m-order reflection that reaches the observation point would contribute the following term to the impulse response:

$$\overset{+}{f}{}_I^{\mathrm{mr}}(t) = E_0^i \overset{+}{R}_M |A_t(s_t)|, \tag{19}$$

where

$$s_t = s_i + \sum_{j=1}^{m} s_r^j,$$

$$A_t(s_t) = A_i(s_i) \prod_{j=1}^{m} A_r\left(s_r^j\right), \tag{20}$$

$$\overset{+}{R}_M = \overset{+}{R}_1\left(t - \frac{s_i}{c} - \frac{s_r^1}{c}\right) * \cdots * \overset{+}{R}_m\left(t - \frac{s_i}{c} - \sum_{i=1}^{m} \frac{s_r^j}{c}\right),$$

with s_r^j being the distance between the jth the $(j+1)$th reflection points (or between the mth reflection point and the observation point in the case of the last reflection).

Analogously, the m-order transmitted field will be

$$\overset{+}{f}{}_I^{\mathrm{mt}}(t) = E_0^i \overset{+}{T}_M |A_t(s_t)|, \tag{21}$$

where $\overset{+}{T}_M(t) = I + \overset{+}{R}_M(t)$.

2.6. Reflected-Diffracted and Diffracted-Reflected Fields. Following the same procedure for multiple reflections, the contribution of the interaction between an edge and a reflecting surface to the impulse response can be written as

$$\overset{+}{f}{}_I^{\mathrm{rd}}(t) = E_0^i \left[\overset{+}{R}\left(t - \frac{s_i}{c} - \frac{s_r}{c}\right) * \overset{+}{D}\left(t - \frac{s_i}{c} - \frac{s_r}{c} - \frac{s_d}{c}\right)\right] \cdot |A_i(s_i) A_r(s_r) A_d(s_d)| \tag{22}$$

for the case of reflection-diffraction interaction and

$$\overset{+}{f}{}_I^{\mathrm{dr}}(t) = E_0^i \left[\overset{+}{D}\left(t - \frac{s_i}{c} - \frac{s_d}{c}\right) * \overset{+}{R}\left(t - \frac{s_i}{c} - \frac{s_r}{c} - \frac{s_d}{c}\right)\right] \cdot |A_i(s_i) A_d(s_d) A_r(s_r)| \tag{23}$$

for the case of diffraction-reflection interaction.

The meaning of these parameters is analogous to the previous effects.

3. The Angular Z-Buffer (AZB) Algorithm

The AZB technique was presented in [5, 14] and is summarized here due to its applicability to the time-domain formulation to reduce the computational cost associated with the analysis of realistic environments. The method consisted of dividing the space from the source point into spherical sectors called anxels. These anxels are defined by the spherical coordinates, theta (θ) and phi (ϕ) for a fixed coordinate system with the origin set at the source.

The anxel belonging to each facet is computed from the spherical coordinates of its vertices. This information is stored in the so-called AZB matrix. This information depends, exclusively, on the source point and on the

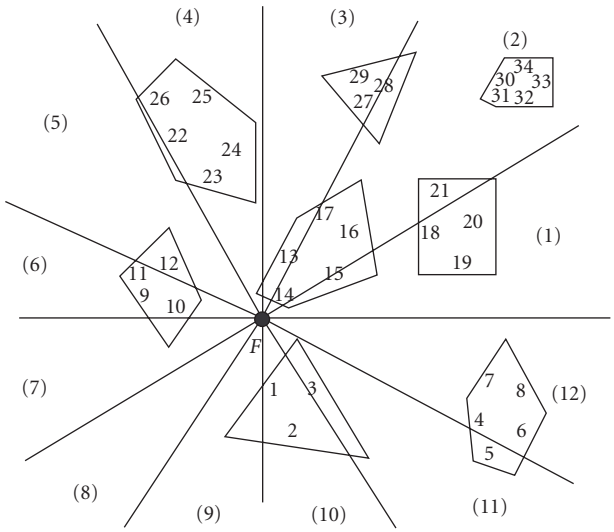

Figure 4: Example of a 2D outdoor scene divided in 12 "anxels".

Table 1: Facets storage in the AZB of the scene of Figure 4.

Anxel	Facets
1	14, 15, 16, 18, 19, 20, 21
2	14, 16, 17, 27, 28, 18, 21, 31, 32, 30, 33, 34
3	14, 13, 17, 27, 29
4	14, 13, 23, 24, 25, 26
5	12, 11, 23, 22, 26
6	10, 12, 9, 11
7	10, 9
8	
9	1, 2
10	1, 2
11	1, 3, 2, 4, 5, 6
12	4, 7, 8, 6

environmental model. The facets of each anxel are sorted according to their distances from the source (S). For instance, Figure 4 shows a simple 2D outdoor scene where a space partitioning in 12 anxels has been accomplished. Table 1 shows the storage of the facets in the AZB matrix. The procedure is easily generalized for the 3D case by including the second spherical coordinate.

To perform the shadowing test for a given observation point (O), O is located in the corresponding anxel by means of its spherical coordinates. Then facets placed in the anxel with distances to S less than the distance S-O are included. This inclusion allows reduction of the computation time for the shadowing test calculation by several orders of magnitude. As this test, as explained in [14], encompassed most of the computational cost of the ray-tracing techniques, the complexity of the analysis in general is drastically reduced by the application of the AZB algorithm.

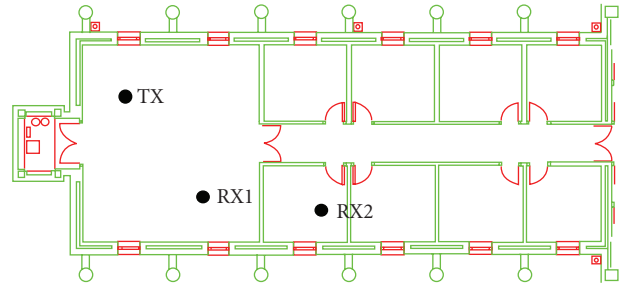

Figure 5: Plant of the Polytechnic Building corridor of the Alcala University and TX and RX placements for the measurement antennas.

Table 2: Electrical characteristics of the materials of the measurements scenario.

Material	ε_r	σ (S/m)
Concrete	4.5	0.01
Wood	2	10^{-5}
Glass	6.5	10^{-12}

4. Discussion of Results and Practical Considerations

The measurements in our experiments have been performed in a complex realistic site to investigate the validity of the approach. The measurements have been done in the corridor of the second floor of the Polytechnic Building of the University of Alcala. Figure 5 shows the plan schematic of the measurement site. The dimensions of the scenario are 7.9×20.7 metres. A 3D plane-facets model has been designed to represent the realistic environment composed of 77 facets. The material composition of the elements of the site was concrete for the walls, wood for the doors and glass for the windows. Table 2 lists the electrical properties of these three materials considered in our model.

Several measurements were performed on the site. Examples of one Line of Sight (LOS) and one Non Line of Sight (NLOS) case will be shown in this section. Figure 5 illustrates the position of the transmitter and the receiver in both cases. The coordinates of the transmitter were (1.60, 5.55, 1.10) and the receivers were (5.0, 1.78, 1.10) for the LOS case and (9.55, 1.3, 1.10) for the NLOS case. All the coordinates are given in metres.

Measurements have been conducted in the frequency domain using the network analyzer (VNA) Agilent E8362B. Two Double-Ridged Waveguide antennas linearly polarized were used as transmitter (TX) and receiver (RX), respectively, similar to the approach in [19]. The frequency range of these antennas was 1 to 18 GHz. In this range, the average VSWR ratio was lower than 1.5.

Figure 6 shows an overview of the measurements setup. The VNA was set to transmit 3201 tones uniformly distributed over the 1–18 GHz frequency range. This gave an excess delay of ~188 ns and a maximum distance of 56.4 m. The temporal resolution for the 17 GHz frequency was 59 ps.

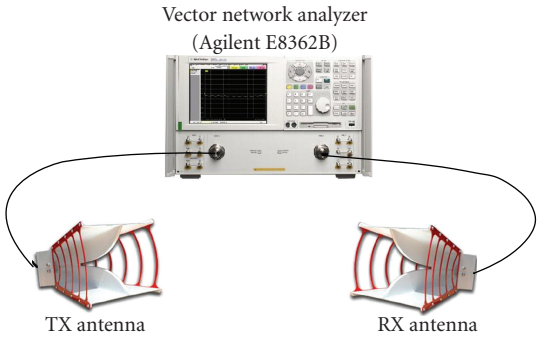

Figure 6: Overview of the measurements setup.

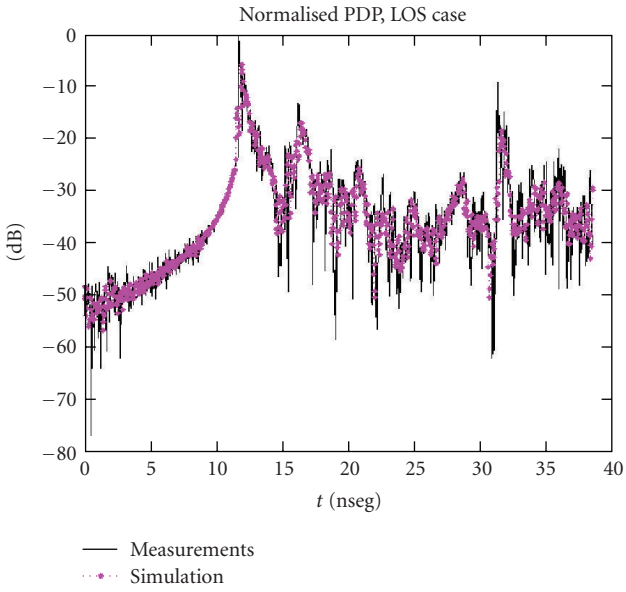

Figure 7: Comparison between measurements and simulation for the LOS case.

The input signal is expressed as a sum of a small number of simple expansion functions for a more efficient convolution with the TD-UTD impulse response. In this approach the input signal is represented as the sum of waveforms whose analytical signal representations are simple poles in the complex-time plane. This representation allows the convolution to be expressed in a closed form, thus speeding up computation. Moreover, in this representation is included the antenna transfer function. Equations (24) and (25) show the representation of the input signal and the closed form for the convolution, respectively:

$$\overset{+}{i}(t) = \frac{j}{\pi}\sum_{n=1}^{n}\frac{A_n}{t + j\tau_n}, \tag{24}$$

$$\overset{+}{o}(t) = \frac{1}{2}\overset{+}{i}(t) * \overset{+}{f}(t) = \sum_{n=1}^{N} A_n \overset{+}{f}(t + j\tau_n). \tag{25}$$

The comparison between the measurements and our approach for the normalized PDP in the LOS and the NLOS cases is shown in Figures 7 and 8, respectively. As

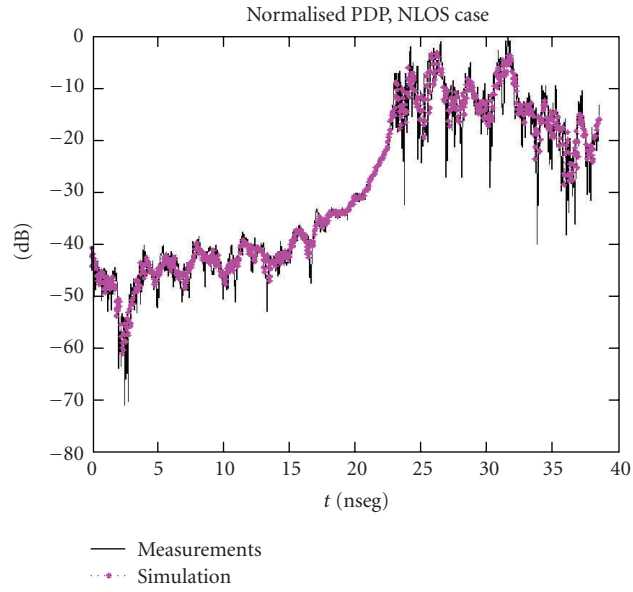

Figure 8: Comparison between measurements and simulation for the LOS case.

can be seen, a good agreement between calculation and measurement is obtained in both cases. The mean errors were only 3.5 dB for the LOS case and 4.6 dB for the NLOS case, which are very good for UWB applications. If the lossy components of the materials are not included the mean errors increase to 7.2 dB and 10.1 dB, respectively. Obviously, neglecting the lossy components in the model decreases the accuracy of the prediction. The computation time was 1 minute 23 seconds. for the LOS case and 1 minute 42 seconds. for the NLOS case considering up to sixth order reflections. Both results were obtained using an AMD Athlon microprocessor at 1.99 GHz. Hence, the method is very suitable for analysing realistic environments at high speed. This high computation speed was due to the combination of the TD-UTD formulation with the AZB ray-tracing acceleration technique. It is important to mention that the computation time includes the creation of the AZB matrices. Therefore, considering that the AZB matrices only have to be created once, the computation time for the NLOS case is only 35 seconds after the computation of the LOS case. Therefore, the calculation of additional point would only take an amount of time of that order of magnitude.

5. Conclusions

An accurate, high-speed method based on TD-UTD to analyze indoor propagation for UWB systems has been presented. The time domain analysis used is especially suitable for the problem under study, but it is also important to include in the TD-UTD formulation the contribution of lossy materials and multiple effects for this kind of analysis. Experimental measurements have been performed at the University of Alcala and the agreement of the presented model with the measured results is excellent. The main advantage of the approach is the possibility of analyzing

UWB propagation in realistic environments in a reasonable amount of time. This advantage is afforded by the combination of the electromagnetic analysis with acceleration ray-tracing techniques such as the AZB algorithm.

Acknowledgments

The University of Alcala team's work has been supported, in part, by the Spanish Department of Education and Science, Project 2006-03140 and by the Program of Mobility of the University of Alcalá. A. S. Mohan's work is supported by a Discovery Project Grant DP 0346540 funded by the Australian Research Council. The Centro de Alta Tecnología y Homologación (CATECHOM) of the University of Alcalá has collaborated in the measurements procedure.

References

[1] A. A. M. Saleh and R. A. Valenzuela, "A statistical model for indoor multipath propagation," *IEEE Journal on Selected Areas in Communications*, vol. 5, no. 2, pp. 128–137, 1987.

[2] S. Y. Seidel and T. S. Rappaport, "914 MHz path loss prediction models for indoor wireless communications in multifloored buildings," *IEEE Transactions on Antennas and Propagation*, vol. 40, no. 2, pp. 207–217, 1992.

[3] A. J. Motley and J. M. Keenan, "Radio coverage in buildings," *British Telecom Technology Journal*, vol. 8, no. 1, pp. 19–24, 1990.

[4] C. Tornevik, J. E. Berg, and F. Lotse, "900 MHz propagation measurements and path loss models for different indoor environments," in *Proceedings of the IEEE Vehicular Technology Conference (VTC '93)*, 1993.

[5] F. Sáez de Adana, O. G. Blanco, I. G. Diego, J. P. Arriaga, and M. F. Cátedra, "Propagation model based on ray tracing for the design of personal communication systems in indoor environments," *IEEE Transactions on Vehicular Technology*, vol. 49, no. 6, pp. 2105–2112, 2000.

[6] G. M. Whitman, K.-S. Kim, and E. Niver, "Theoretical model for radio signal attenuation inside buildings," *IEEE Transactions on Vehicular Technology*, vol. 44, no. 3, pp. 621–629, 1995.

[7] J. H. Tarng, W. R. Chang, and B. J. Hsu, "Three-dimensional modelling of 900 MHz and 2.44 GHz radio propagation in corridors," *IEEE Transactions on Vehicular Technology*, vol. 46, pp. 519–526, 1997.

[8] A. Lauer, A. Bahr, and I. Wolff, "FDTD simulations of indoor propagation," in *Proceedings of the 44th IEEE Vehicular Technology Conference (VTC '84)*, pp. 875–878, 1984.

[9] R. G. Kouyoumjian and P. H. Pathak, "A uniform geometrical theory of diffraction for an edge in a perfectly conducting surface," *Proceedings of the IEEE*, vol. 62, no. 11, pp. 1448–1461, 1974.

[10] D. Cassioli, M. Z. Win, and A. F. Molisch, "A statistical model for the UWB indoor channel," in *Proceedings of the 53rd IEEE Vehicular Technology Conference (VTC '01)*, vol. 2, pp. 1159–1163, May 2001.

[11] A. Molisch, D. Cassioli, C. Chong, et al., "A comprenhensive standardized model for ultrawideband propagation channels," *IEEE Transactions on Antennas and Propagation*, vol. 54, pp. 3151–3166, 2006.

[12] T. Vemttipong and R. G. Kouyoumjian, "Early-time responses of currents and charges on wedges and strips," in *Proceedings of the IEEE APS International Symposium on Antennas and Propagation*, pp. 590–593, 1979.

[13] P. R. Rousseau and P. H. Pathak, "Time-domain uniform geometrical theory of diffraction for a curved wedge," *IEEE Transactions on Antennas and Propagation*, vol. 43, no. 12, pp. 1375–1382, 1995.

[14] M. F. Cátedra, J. Pérez, F. Sáez de Adana, and O. Gutierrez, "Efficient ray-tracing techniques for 3D analysis of propagation in mobile communications. Application to picocell and microcell scenarios," *IEEE Antennas and Propagation Magazine*, vol. 40, no. 2, pp. 15–27, 1998.

[15] R. Yao, W. Zhu, and Z. Chen, "An efficient time-domain ray model for UWB indoor multipath propagation channel," in *Proceedings of the 58th IEEE Vehicular Technology Conference (VTC '03)*, pp. 1293–1297, Orlando, Fla, USA, October 2003.

[16] R. Yao, Z. Chen, and Z. Guo, "An efficient multipath channel model for UWB home networking," in *Proceedingsof the IEEE Radio and Wireless Conference (RAWCON '04)*, pp. 511–516, 2004.

[17] A. M. Attiya and A. Safaai-Jazi, "Simulation of ultra-wideband indoor propagation," *Microwave and Optical Technology Letters*, vol. 42, no. 2, pp. 103–108, 2004.

[18] W. Yang, Z. Naitong, Z. Qinyu, and Z. Zhongzhao, "Deterministic simulation of UWB indoor propagation channel," *Journal of Systems Engineering and Electronics*, vol. 19, no. 3, pp. 447–452, 2008.

[19] http://www.ets-lindgren.com/pdf/3115.pdf.